SPECIAL TOPIC — Silicene

Comparison of electronic structure between monolayer silicenes on Ag (111)*

Chun-Liang Lin[a)†], Ryuichi Arafune[b)], Maki Kawai[a)], and Noriaki Takagi[a)‡]

[a)] Department of Advanced Materials Science, Graduate School of Frontier Science, The University of Tokyo, 5-1-5 Kashiwa, Chiba 277-8561, Japan
[b)] International Center for Materials Nanoarchitectonics (WPI-MANA), National Institute for Materials Science, 1-1 Namiki, Ibaraki 304-0044, Japan

(Received 25 February 2015; revised manuscript received 25 May 2015; published online 20 July 2015)

The electronic structures of monolayer silicenes (4×4 and $\sqrt{13}\times\sqrt{13}$R13.9°) grown on Ag (111) surface are studied by scanning tunneling spectroscopy (STS) and density functional theory (DFT) calculations. While both phases have similar electronic structures around the Fermi level, significant differences are observed in the higher energy unoccupied states. The DFT calculations show that the contributions of Si $3p_z$ orbitals to the unoccupied states are different because of their different buckled configurations.

Keywords: silicene, electronic structure, STM, DFT

PACS: 73.22.–f, 68.37.Ef, 61.46.–w, 81.05.Zx **DOI:** 10.1088/1674-1056/24/8/087307

1. Introduction

Silicene, the two-dimensional (2D) honeycomb lattice of Si atoms, has received a lot of attention because it shares remarkable properties with graphene. Density functional theory (DFT) calculations[1,2] have demonstrated that freestanding silicene takes a buckled structure where two Si atoms in the unit cell are displaced in the opposite directions perpendicular to the basal plane. In spite of the buckling, silicene hosts Dirac fermions similarly to graphene. The combination of the Dirac fermion characteristics with sizable spin-orbital coupling (SOC) of Si adds exotic properties to silicene.[3–6] An energy gap opens at the Dirac cone where two linear bands cross at the Fermi level, and topologically protected states emerge at the edges of 2D silicene. This indicates that silicene is promising as a material for realizing the theoretical prediction of Kane and Mele.[7] Besides, silicene is expected to be compatible with the current process technologies to fabricate electronic devices on Si platform.

In the last few years, silicene has not been only in the theoretical calculation; it has successfully been synthesized on many different substrates, such as Ag (110),[8] Ag (111),[9–11] Ir (111),[12] ZrB_2-covered Si (111),[13] and MoS_2 crystal,[14] of which, the silicene synthesized on Ag (111) is investigated most.[9–11,15–39] Several phases such as 4×4, $\sqrt{13}\times\sqrt{13}$R13.9°, $4/\sqrt{3}\times4/\sqrt{3}$, etc. are observed by using low-energy electron diffraction (LEED) and scanning tunneling microscopy (STM). For some of them, the structural models consisting of buckled honeycomb lattice have been proposed.[9–11,15–21] Although it has been proved that Dirac fermions disappear in the monolayer silicene on the Ag (111) surface due to the strong hybridization with the Ag (111) substrate,[25–28,36–39] theoretical calculations predicted that the Dirac fermion characteristics can be preserved in some structures of silicene after they have been extracted from the Ag (111) substrate.[27,33,34] Recently, a field effect transistor (FET) has been fabricated by transferring silicene from Ag (111) to an Al_2O_3/SiO_2 substrate.[40] Since various different monolayer phases appear on Ag (111) surface, it is of great importance to reveal the electronic structures of silicenes in different configurations if they are used in the devices. In this paper, we compare the electronic structures of two dominant phases, 4×4 and $\sqrt{13}\times\sqrt{13}$R13.9°, based on the results acquired by both scanning tunneling spectroscopy (STS) and DFT calculations.

2. Experiment

The whole experiments were performed in an ultra-high vacuum chamber with a base pressure less than 1×10^{-10} Torr (1 Torr = 1.33322×10^2 Pa). To grow silicene on Ag (111) substrate, Si atoms were deposited onto the clean Ag (111) substrate in a constant rate of 0.03 ML/min (1 ML = 1×10^{15} atoms·cm^{-2}) from a heated (> 1100 °C) Si wafer. The Ag (111) substrate was cleaned by repeated cycles of Ar^+ sputtering and annealing at 500 °C. The trick to crystalize sil-

*Project supported by the Ministry of Education, Culture, Sports, Science and Technology (MEXT) through Grants-in-Aid for Scientific Research (Grant Nos. 24241040 and 25110008) and the World Premier International Research Center Initiative (WPI), MEXT, Japan.

†Corresponding author. E-mail: clin@ams.k.u-tokyo.ac.jp
‡Corresponding author. E-mail: n-takagi@k.u-tokyo.ac.jp

© 2015 Chinese Physical Society and IOP Publishing Ltd

icene is the precise control of the Ag (111) substrate temperature. In our experiments, the temperature was kept at 260 °C during the deposition. After sample preparation, the STM and STS measurements were carried out at 6 K.

The DFT calculations were carried out by the plane-wave-based Vienna *Ab initio* Simulation Package (short as VASP)[41,42] with the projected augmented wave (PAW)[43] potentials in the generalized gradient approximation (GGA). The exchange–correlation functional of Perdew–Burke–Ernzerhof (PBE)[44] was used. The kinetic-energy cutoff for the plane-wave basis was set to be 400 eV. The silicene grown on Ag (111) was modeled by using a supercell, which consists of a silicene layer on a 5-layer Ag slab with a vacuum of ~18 Å thick along the surface normal. The supercell used for the 4×4 ($\sqrt{13}\times\sqrt{13}$R13.9°) phase was composed of 80 Ag and 18 Si (65 Ag and 18 Si) atoms. The atoms in the bottom two layers were fixed at their ideal bulk positions during the structure optimization. The positions of atoms in silicene and top three layers of the Ag slab were optimized without any constraint until the forces on individual atoms were less than 0.01 eV/Å. In the self-consistent total energy calculations, the Brillouin zone was sampled with $(5\times5\times1)$ k-points.

3. Results and discussion

Figure 1(a) shows an STM image of monolayer silicene grown on Ag (111). Both 4×4 and $\sqrt{13}\times\sqrt{13}$R13.9° phases coexist on the surface. A zoom-in image of the green square in Fig. 1(a) is shown in Fig. 1(b). Taking a careful look at the high-resolution image on the left side of the image, one can see six protrusions and a darker hole in the unit cell. This feature indicates that the left side is attributed to the 4×4 phase. On the right side separated by a domain boundary, $\sqrt{13}\times\sqrt{13}$R13.9° phase appears. The angle difference between two phases is ~ 14° as indicated by the black and blue arrows.

Figure 1(c) shows the typical STS spectra acquired on 4×4 and $\sqrt{13}\times\sqrt{13}$R13.9° phases. The spectra are obtained by a lock-in technique with a modulation voltage of 4 mV at 512 Hz added to the sample voltage. The spectra do not show strong dependence on the position inside the unit cell. The spectrum of 4×4 phase is similar to that of $\sqrt{13}\times\sqrt{13}$R13.9° phase. Two spectra almost overlap each other in the range from −1.0 V to 0.5 V. A difference is observed in the range from 0.5 V to 1.0 V; the intensity of 4×4 phase is stronger than that of $\sqrt{13}\times\sqrt{13}$R13.9° phase. We consider that this difference is minor and the electronic structures of 4×4 and $\sqrt{13}\times\sqrt{13}$R13.9° phases are essentially analogous around the Fermi level.

In contrast, the unoccupied electronic states in higher energy range are different. Figure 1(d) shows the dZ/dV spectra acquired in a bias range from 1.0 V to 3.8 V. In the

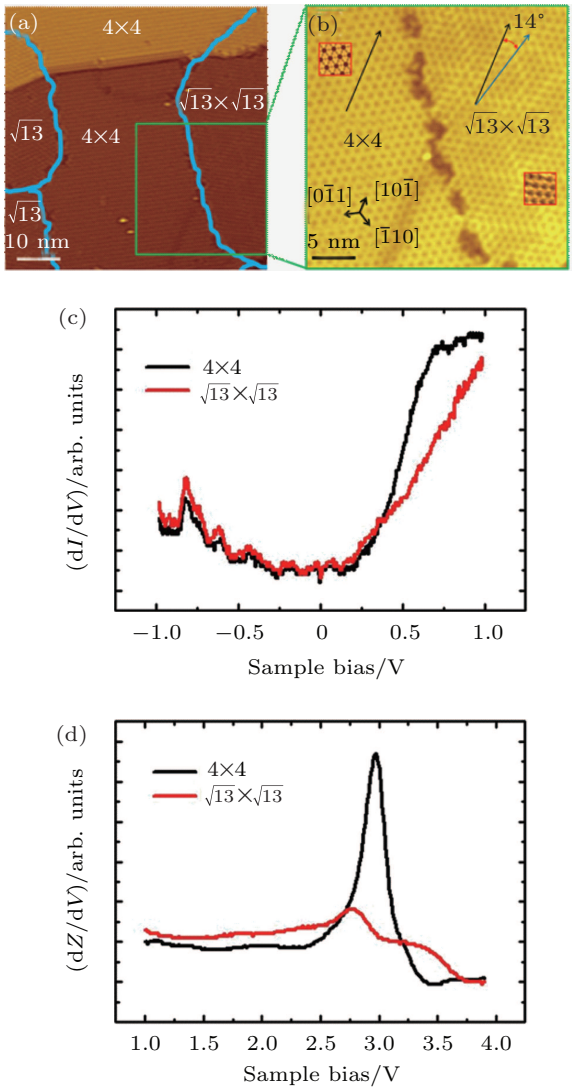


Fig. 1. (color online) (a) Topographic STM image of monolayer silicene on Ag (111) at a sample bias of $V_s = 0.5$ V and tunneling current of $I_t = 0.2$ nA. The image size is 60 nm×60 nm. Both 4×4 and $\sqrt{13}\times\sqrt{13}$R13.9° phases coexist on the surface. The blue curves indicate the domain boundaries. (b) The zoom-in image of the green square in panel (a) with $V_s = 0.5$ V, $I_t = 0.2$ nA, and size is 30 nm×30 nm. The 4×4 phase matches the symmetry axes of the Ag (111) substrate while the $\sqrt{13}\times\sqrt{13}$R13.9° phase rotates an angle of 14°. High resolution images (3.5 nm×3.5 nm, $V_s = -0.02$ V, and $I_t = 0.2$ nA) of defined areas are attached in the image. (c) dI/dV spectra and (d) dZ/dV spectra of the 4×4 and $\sqrt{13}\times\sqrt{13}$R13.9° phases taken by a lock-in technique. The modulation voltages of panel (c) 4 mV at 512 Hz and panel (d) 14 mV at 512 Hz are added to the sample voltage in the lock-in measurements.

Z–V spectrum, the displacement of the tip (Z) is measured as a function of bias voltage (V) applied to the STM junction with holding the feedback loop on. The tip promptly retracts from the surface to keep the tunneling current constant when the density of states increases at certain voltages. In other words, the displacement of the tip depends on how the density of states varies with energy. By differentiating the Z–V curve, peaks appear at the voltages where the density of states is relatively high. Therefore, the dZ/dV spectrum is basically proportional to the density of states; it reveals the electronic structure as well as the conventional STS spectrum.[45–47] The spectra shown here are obtained by a lock-in technique with a

modulation voltage of 14 mV at 512 Hz. A sharp peak appears at 2.95 V in 4×4 phase while a broad peak around 2.70 V and a shoulder near 3.40 V are observed for $\sqrt{13}\times\sqrt{13}$R13.9° phase. These spectral signatures show the difference in electronic structures between the two phases.

To understand the variations in the electronic structures of two phases, the electronic band structures are calculated for both 4×4 and $\sqrt{13}\times\sqrt{13}$R13.9° phases. The calculated band structures of 4×4 and $\sqrt{13}\times\sqrt{13}$R13.9° phases are shown in Figs. 2(a) and 2(b), respectively. The contribution of Si $3p_z$ orbital is indicated by the gradient bar. The higher contribution appears in darker colors. The Brillouin zone (BZ) of each structure is shown in Figs. 2(c) and 2(d). Note that the K point (K_1) in the BZ of silicene 1×1 overlaps with the Γ point (Γ_2) in the extended BZs of 4×4 or $\sqrt{13}\times\sqrt{13}$R13.9° phases. Thus the band structures in Figs. 2(a) and 2(b) are drawn along the high symmetry directions in the BZs. Both band structures become complicated because of the following reasons. (i) The bulk bands are discretized because we describe the system as a slab model. Although the bulk Ag bands essentially should appear as a background, they appear as many branches to overlap with the bands derived from Si. (ii) The bands relevant to the Si $3p_z$ orbital hybridize with the substrate Ag states and their contributions are scattered.

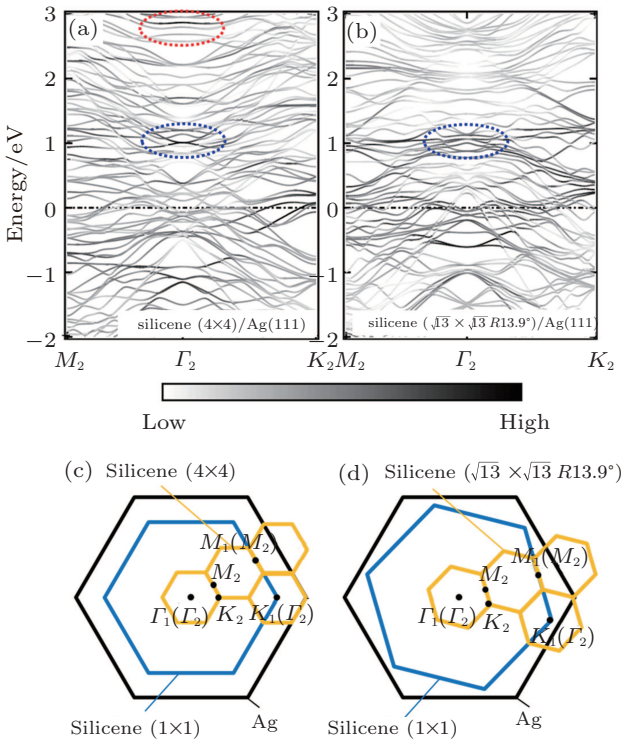


Fig. 2. (color online) Calculated band structures of (a) 4×4 and (b) $\sqrt{13}\times\sqrt{13}$R13.9°. The gradient bar manifests the contribution of Si $3p_z$ orbital to each branch. The darker the region, the higher the contribution in the region is. Panels (c) and (d) indicate the Brillouin zones (BZs) of 4×4 and $\sqrt{13}\times\sqrt{13}$R13.9° phases together with the BZs of Ag (111) 1×1 and silicene 1×1. The yellow hexagons in panels (c) and (d) represent the BZs of 4×4 and $\sqrt{13}\times\sqrt{13}$R13.9° phases, respectively. The blue hexagons refer to the BZs of corresponding 1×1 honeycomb lattice in each structure. The black hexagons denote the BZs of the Ag (111) surface. Γ_1, K_1, and M_1 are the highly symmetric points in the BZ of silicene 1×1 and Γ_2, K_2, and M_2 are the highly symmetric points in the BZ of 4×4 or $\sqrt{13}\times\sqrt{13}$R13.9°.

The band structures of the 4×4 and $\sqrt{13}\times\sqrt{13}$R13.9° phases are essentially similar especially near the Fermi level. The Dirac cone feature observed for the freestanding silicene disappears for both phases. The Ag (111) surface has a band gap extending between −0.4 eV and 3.9 eV from the lower to the upper sp-band.[48–50] Although the band gap opens at the Fermi level, the lower sp-band is distributed near the Fermi level so that it strongly hybridizes with the Si $3p_z$ orbital. The hybridization strikingly reduces the contribution of Si $3p_z$ orbital near the Fermi level. Although the Dirac cone feature observed for the freestanding silicene should appear at the Γ_2 point for both phases, it cannot be found in Fig. 2(a) nor in Fig. 2(b). Near the Γ_2 point, the bands derived from Si $3p_z$ orbital contribute at 1 eV above the Fermi level in both 4×4 and $\sqrt{13}\times\sqrt{13}$R13.9° phases as marked by the blue circles in Figs. 2(a) and 2(b). These features are matched with the increase of spectral intensity near 1 eV above the Fermi level in the STS spectra as shown in Fig. 1(c).

One can easily see the difference in band structure between the 4×4 and $\sqrt{13}\times\sqrt{13}$R13.9° phases. The contributions of Si $3p_z$ orbital almost disappear for the energy above 1 eV in the $\sqrt{13}\times\sqrt{13}$R13.9° phase but several bands generated by Si $3p_z$ orbital appear near 3 eV above the Fermi level in the 4×4 phase as marked by the red circle in Fig. 2(a). This difference between the band structures can help us explain the huge diversity found in the dZ/dV spectra. A peak near 3 eV above the Fermi level is found on the 4×4 phase as shown in Fig. 1(d). In contrast, the spectrum of the $\sqrt{13}\times\sqrt{13}$R13.9° phase is relatively broad because most of the bands near 3 eV come from the Ag substrate. The striking difference in electronic structure, originating from the different buckled configurations, is observed in the higher energy regions. This is also solid evidence to show that the different structures of silicene grown on Ag (111) are not moiré patterns, in contrast to other honeycomb lattices on metal substrates such as graphene on Ir (111),[51] Pt (111),[52] Ru (0001),[53] Cu (111),[54] and h-BN on Cu (111)[55]. The moiré patterns can be observed due to the mismatch between the overlayers and the substrate lattices. For example, two kinds of moiré patterns with different periodicities are observed for graphene on Cu (111) surface while rotating the graphene lattice 7° with respect to the Cu (111) lattice.[54] In the case of silicene on Ag (111), it is more than the rotations of a honeycomb lattice; in fact different phases reveal different buckled configurations. The electronic structures of silicene seriously correlate with their own geometric configurations.

The difference in geometric configuration between 4×4 and $\sqrt{13}\times\sqrt{13}$R13.9° phases is briefly described below based

on our structural models. Figures 3(a) and 3(b) show calculated STM images together with the STM observations of 4×4 and $\sqrt{13}\times\sqrt{13}$R13.9° phases, respectively. The yellow rhombuses in the middle indicate the unit cell of each phase. The simulated images reasonably agree with the real STM images, and thus the models of these two structures shown below should be very close to the real structures. The models of the 4×4 and $\sqrt{13}\times\sqrt{13}$R13.9° phases are shown in Figs. 3(c) and 3(d), respectively. Although both 4×4 and $\sqrt{13}\times\sqrt{13}$R13.9° phases consist of the same number of Si atoms (18 Si atoms in each unit cell), the cell size and the buckled configuration are so different: the cell sizes of the 4×4 and $\sqrt{13}\times\sqrt{13}$R13.9° phases are 11.56 Å and 10.42 Å, respectively. From the side view of each structural model shown in Figs. 3(e) and 3(f), it is obvious that the buckled configurations in two phases are different. The $\sqrt{13}\times\sqrt{13}$R13.9° phase takes a typical buckled configuration where the number of upper Si atoms in the unit cell is equal to that of lower Si atoms, while the 4×4 phase is another scenario. The structural parameters of these two models are listed in Table 1. It is not difficult to find that Si slightly adjusts its bond length under different conditions. For example, the bond lengths of Si–Si in 4×4 phase range from 2.29 Å to 2.31 Å which have been

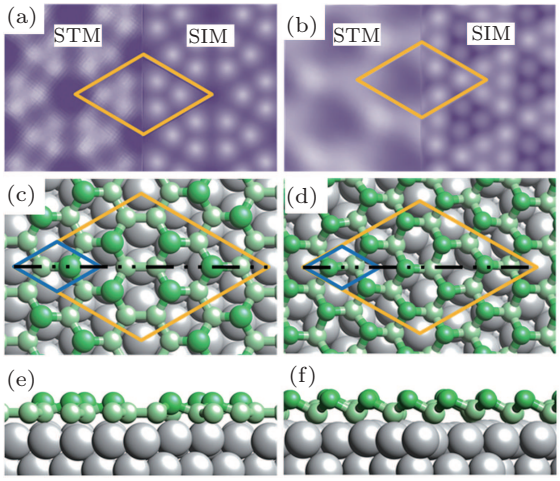


Fig. 3. (color online) (a) and (b) Simulated STM images (SIM) combined with the real STM images of the 4×4 and $\sqrt{13}\times\sqrt{13}$R13.9° phases, respectively. Structural models of (c) 4×4 and (d) $\sqrt{13}\times\sqrt{13}$R13.9° phases optimized by the DFT calculations. The unit cell of each model is indicated by yellow rhombus and the small blue rhombuses indicate the corresponding 1×1 unit cells. (e) and (f) the side views of each model.

Table 1. Structural parameters of the 4×4 and $\sqrt{13}\times\sqrt{13}$R13.9° phases: sizes of unit cell, the variation of Si–Si bond lengths, the height difference between the highest and lowest Si atoms, and the variation of buckling angles.

Structure	4×4	$\sqrt{13}\times\sqrt{13}$R13.9°
Unit cell	11.56 Å	10.42 Å
Si–Si bond	2.29 Å∼2.31 Å	2.29 Å
Si–Ag distance	2.56 Å	2.14 Å
Height difference	0.7 Å	1.0 Å
Buckling angle	95°∼109°	118°

determined by the tensor LEED analysis.[30] They are different from the value of 2.29 Å in $\sqrt{13}\times\sqrt{13}$R13.9° phase. Therefore, different phases of silicene on Ag (111) are caused not only by the rotation of silicene lattice but also by the modification in the Si–Si bonds. The electronic structures therefore drastically change between the two structures.

Before closing discussion, we come to discuss the geometric structure of $\sqrt{13}\times\sqrt{13}$R13.9°. Up to now, at least five models have been proposed by different calculations. We have proposed a typical buckled model as shown in Fig. 3(d). Jamgotchian *et al.*[15] and Enriquez *et al.*[16] have proposed two similar models. Other two models have been recently proposed by Pflugradt *et al.*[33] A very recent STM observation done by Liu *et al.*[56] shows that the STM images match the model proposed by Jamgotchian *et al.* and Enriquez *et al.* Nevertheless, except for our model, the other models contain 14 Si atoms in the unit cell. These models provide an Si density of 1.077 Si atoms per Ag (111) 1×1 unit cell, which is lower than that of the 4×4 phase (1.125 Si atoms per Ag (111) 1×1 unit cell). In the LEED observation, the $\sqrt{13}\times\sqrt{13}$R13.9° phase usually appears in higher coverage regime after the 4×4 phase has been formed.[19,29] It is more convincing if the $\sqrt{13}\times\sqrt{13}$R13.9° phase consists of a higher density of Si than the 4×4 phase. Since our model contains 18 Si atoms in the unit cell of the $\sqrt{13}\times\sqrt{13}$R13.9° phase, the Si density is 1.385 Si atoms per Ag (111) unit cell. This value is higher than that of the 4×4 phase and agrees with most of LEED observations. Besides, the electronic structure calculated from our model is nearly consistent with our STS and dZ/dV observations while the electronic structures[33,35] calculated for the other models[15,16,35] hardly explain the current STS and dZ/dV results.

4. Conclusions

Silicene has been acknowledged as a new allotrope of Si. Comparing with graphene, silicene is more flexible in structure. Different buckled configurations are found from the silicene synthesized on Ag (111) surface. By the combination of STS measurements and DFT calculations, we successfully find the difference in electronic structure between the 4×4 and $\sqrt{13}\times\sqrt{13}$R13.9° phases, which arises from the different buckling configurations. In the STS measurement, similar spectra found near the Fermi level are regarded as a consequence of the hybridization with Ag (111). The metal substrate affects the electronic structure near the Fermi level. However, a sharp peak appears at 2.95 V, far from the Fermi level, in the 4×4 phase whereas it is not observed in the $\sqrt{13}\times\sqrt{13}$R13.9° phase. This difference originates from the different buckled configurations in the honeycomb lattice. This is verified with the DFT calculations; much stronger con-

tribution of Si $3p_z$ orbital is found in the 4×4 phase than in the $\sqrt{13} \times \sqrt{13}$R13.9° phase above 3 eV from the Fermi level.

Acknowledgement

Computation in this work was performed by using the facilities of the Supercomputer Center, the Institute for Solid State Physics, University of Tokyo.

References

[1] Takeda K and Shiraishi K 1994 *Phys. Rev. B* **50** 14916
[2] Cahangirov S, Topsakal M, Aktrük E, Sahin H and Ciraci S 2009 *Phys. Rev. Lett.* **102** 236804
[3] Liu C C Feng W and Yao Y 2011 *Phys. Rev. Lett.* **107** 076802
[4] Ezawa M 2012 *J. Phys. Soc. Jpn.* **81** 064705
[5] Ezawa M 2012 *Phys. Rev. Lett.* **109** 055502
[6] Drummond N D, Zólyomi V and Fal'ko V I 2012 *Phys. Rev. B* **85** 075423
[7] Kane C L and Mele E J 2005 *Phys. Rev. Lett.* **95** 226801
[8] De Padova P, Quaresima C, Ottaviani C, Sheverdyaeva P M, Moras P, Carbone C, Olivieri D T B, Kara A, Oughaddou H, Aufray B, and Le Lay G 2010 *Appl. Phys. Lett.* **96** 261905
[9] Lalmi B, Oughaddou H, Enriquez H, Kara A, Vizzini S, Ealet B and Aufray B 2010 *Appl. Phys. Lett.* **97** 223109
[10] Lin C L, Arafune R, Kawahara K, Tsukahara N, Minamitani E, Kim Y, Takagi N and Kawai M 2012 *Appl. Phys. Express* **5** 045802
[11] Vogt P, De Padova P, Quaresima C, Avila J, Frantzeskakis E, Asensio M C, Resta A, Ealet B and Le Lay G 2012 *Phys. Rev. Lett.* **108** 155501
[12] Meng L, Wang Y, Zhang L, Du S, Wu R, Li L, Zhang Y, Li G, Zhou H, Hofer W A and Gao H 2013 *Nano Lett.* **13** 685
[13] Fleurence A, Friedlein R, Ozaki T, Kawai H, Wang Y and Yamada-Takamura Y 2012 *Phys. Rev. Lett.* **108** 245501
[14] Chiappe D, Scalise E, Cinquanta E, Grazianetti C, van den Broek B, Fanciulli M, Houssa M and Molle A 2014 *Adv. Mater.* **26** 2096
[15] Jamgotchian H, Colignon Y, Hamzaoui N, Ealet B, Hoarau J Y, Aufray B and Bibérian J P 2012 *J. Phys.: Condens. Matter* **24** 172001
[16] Enriquez H, Vizzini S, Kara A, Lalmi B and Oughaddou H 2012 *J. Phys.: Condens. Matter* **24** 314211
[17] Feng B, Ding Z, Meng S, Yao Y, He X, Cheng P, Chen L and Wu K 2012 *Nano Lett.* **12** 3507
[18] Chen L, Liu C C, Feng B, He X, Cheng P, Ding Z, Meng S, Yao Y and Wu K 2012 *Phys. Rev. Lett.* **109** 056804
[19] Arafune R, Lin C L, Kawahara K, Tsukahara N, Minamitani E, Kim Y, Takagi N and Kawai M 2013 *Surf. Sci.* **608** 297
[20] Cinquanta E, Scalise E, Chiappe D, Grazianetti C, van den Broek B, Houssa M, Fanciulli M and Molle A 2013 *J. Phys. Chem. C* **117** 16719
[21] Fukaya Y, Mochizuki I, Maekawa M, Wada K, Hyodo T, Matsuda I and Kawasuso A 2013 *Phys. Rev. B* **88** 205413
[22] Chen L, Liu C C, Feng B, He X, Cheng P, Ding Z, Meng S, Yao Y and Wu K 2013 *Phys. Rev. Lett.* **110** 229702
[23] De Padova P, Vogt P, Resta A, Avila J, Razado-Colambo I, Quaresima C, Ottaviani C, Olivieri B, Bruhn T, Hirahara T, Shirai T, Hasegawa S, Asensio M C and Le Lay G 2013 *Appl. Phys. Lett.* **102** 163106
[24] De Padova P, Avila J, Resta A, Razado-Colambo I, Quaresima C, Ottaviani C, Olivieri B, Bruhn T, Vogt P, Asensio M C and Le Lay G 2013 *J. Phys.: Condens. Matter* **25** 382202
[25] Lin C L, Arafune R, Kawahara K, Kanno M, Tsukahara N, Minamitani E, Kim Y, Kawai M and Takagi N 2013 *Phys. Rev. Lett.* **110** 076801
[26] Arafune R, Lin C L, Nagao R, Kawai M and Takagi N 2013 *Phys. Rev. Lett.* **110** 229701
[27] Wang Y P and Cheng H P 2013 *Phys. Rev. B* **87** 245430
[28] Cahangirov S, Audiffred M, Tang P, Iacomino A, Duan W, Merino G and Rubio A 2013 *Phys. Rev. B* **88** 035432
[29] Moras P, Mentes T O, Sheverdyaeva P M, Locatelli A and Carbone C 2014 *J. Phys.: Condens. Matter* **26** 185001
[30] Kawahara K, Shirasawa T, Arafune R, Lin C L, Takahashi T, Kawai M and Takagi N 2014 *Surf. Sci.* **623** 25
[31] Sone J, Yamagami T, Aoki Y, Nakatsuji K and Hirayama H 2014 *New J. Phys.* **16** 095004
[32] Shirai T, Shirasawa T, Hirahara T, Fukui N, Takahashi T and Hasegawa S 2014 *Phys. Rev. B* **89** 241403
[33] Pflugradt P, Matthes L and Bechstedt F 2014 *Phys. Rev. B* **89** 035403
[34] Scalise E, Cinquanta E, Houssa M, van den Broek B, Chiappe D, Grazianetti C, Pourtois G, Ealet B, Molle A, Fanciulli M, Afanas'ev V V and Stesmans A 2014 *Appl. Surf. Sci.* **291** 113
[35] Tchalala M R, Enriquez H, Yildirim H, Kara A, Mayne A J, Dujardin G, Ali M A and Oughaddou H 2014 *Appl. Surf. Sci.* **303** 61
[36] Yuan Y, Quhe R, Zheng J, Wang Y, Ni Z, Shi J and Lu J 2014 *Physica E* **58** 38
[37] Mahatha S K, Moras P, Bellini V, Sheverdyaeva P M, Struzzi C, Petaccia L and Carbone C 2014 *Phys. Rev. B* **89** 201416
[38] Stephan R, Hanf M C and Sonnet P 2015 *J. Phys.: Condens. Matter* **27** 015002
[39] Ishida H, Hamamoto Y, Morikawa Y, Minamitani E, Arafune R and Takagi N 2015 *New J. Phys.* **17** 015013
[40] Tao L, Cinquanta E, Chiappe D, Grazianetti C, Fanciulli M, Dubey M, Molle A and Akinwande D 2015 *Nat. Nanotechnol.* **10** 227
[41] Kresse G and Furthmüller J 1996 *Phys. Rev. B* **56** 11169
[42] Kresse G and Furthmüller J 1996 *Comput. Mater. Sci.* **6** 15
[43] Blöchl P E 1994 *Phys. Rev. B* **24** 17953
[44] Perdew J P, Burke K and Ernzerhof M 1996 *Phys. Rev. Lett.* **77** 3865
[45] Feng M, Zhao J and Petek H 2008 *Science* **320** 359
[46] Yang M C, Lin C L, Su W B, Lin S P, Lu S M, Lin H Y, Chang C S, Hsu W K and Tsong T T 2009 *Phys. Rev. Lett.* **102** 196102
[47] Lin C L, Yang M C, Su W B, Lin S P, Lu S M, Lin H Y, Chang C S, Fu T Y and Tsong T T 2010 *Chin. J. Phys.* **48** 855
[48] Miller T, McMahon W E and Chiang T C 1996 *Phys. Rev. Lett.* **77** 1167
[49] Pontius N, Sametoglu V and Petek H 2005 *Phys. Rev. B* **72** 115105
[50] Winkelmann A, Sametoglu V, Zhao J, Kubo A and Petek H 2007 *Phys. Rev. B* **76** 195428
[51] N'Diaye A T, Bleikamp S, Feibelman P J and Michely T 2006 *Phys. Rev. Lett.* **97** 215501
[52] Sutter P, Sadowski J T and Sutter E 2009 *Phys. Rev. B* **80** 245411
[53] Vázquez de Parga A L, Calleja F, Borca B, Passeggi M C G, Hinarejos J J, Guinea F and Miranda R 2008 *Phys. Rev. Lett.* **100** 056807
[54] Gao L, Guest J R and Guisinger N P 2010 *Nano Lett.* **10** 3512
[55] Joshi S, Ecija D, Koitz R, Iannuzzi M, Seitsonen A P, Hutter J, Sachdev H, Vijayaraghavan S, Bischoff F, Seufert K, Barth J V and Auwärter W 2012 *Nano Lett.* **12** 5821
[56] Liu Z L, Wang M X, Xu J P, Ge J F, Le Lay G, Vogt P, Qian D, Gao C L, Liu C and Jia J F 2014 *New J. Phys.* **16** 075006